Powder Technology 322 (2017) 214–225

Contents lists available at ScienceDirect

Powder Technology

journal homepage: www.elsevier.com/locate/powtec

Assessment of chromite liberation spectrum on microscopic images by means of a supervised image classification

Mahmut Camalan [a,*], Mahmut Çavur [b], Çetin Hoşten [a]

[a] Department of Mining Engineering, Middle East Technical University, Ankara, Turkey
[b] Management Information System, Kadir Has University, Istanbul, Turkey

ARTICLE INFO

Article history:
Received 22 May 2017
Received in revised form 18 August 2017
Accepted 27 August 2017
Available online 2 September 2017

Keywords:
Mineral liberation
Optical microscope
Random forest tree
Image classification
Mineral liberation analyzer

ABSTRACT

Assessment of mineral liberation spectrum with all its aspects is essential for plant control and optimization. This paper aims to estimate 2D mineral map and its associated liberation spectrum of a particular chromite sample from optical micrographs by using Random Forest Classification, a powerful machine-learning algorithm implemented on a user-friendly and an open-source software. This supervised classification method can be used to accurately generate 2D mineral map of this chromite sample. The variation of the measured spectra with the sample size is studied, showing that images of 200 particles randomly selected from the optical micrographs are sufficient to reproduce liberation spectrum of this sample. In addition, the 2D spectrum obtained with this classification method is compared with the one obtained from the Mineral Liberation Analyzer (MLA). Although 2D mineralogical compositions obtained by the two methods are quite similar, microscopic analysis estimates poorer liberation than MLA due to the residual noise (misclassified gangue) generated by the classification. Nevertheless, we cannot compare the reliabilities of the two methods, as there is not a standard produce yet to quantify the accuracy of MLA analysis.

1. Introduction

Mineral liberation by size reduction can be defined as the physical detachment of valuable minerals from gangue minerals so that they can be separated at downstream beneficiation stages. Assessment of mineral liberation is important for control and optimization of grinding and downstream separation circuits [1–6]. One approach for the assessment of mineral liberation is to estimate the degree of liberation through mathematical models simulating random or non-random breakage events [7–11]. However, these models have not been applied commonly in commercial softwares simulating mineral processing circuits [12]. Besides, knowing only the degree of liberation may not be sufficient for the process mineralogy because the degree of liberation represents a single point of the liberation spectrum [13]. Therefore, more quantitative data regarding the morphological and compositional properties, i.e. mineralogical maps, of progeny particles should be collected. Mineral liberation spectrum or distribution, in this respect, is the abundance and grade distribution of a selected mineral phase in a population of progeny particles varying in size [11,12,14–17]. The spectrum with its associated mineralogical map are particularly used in the fields of process mineralogy [1–3,18–21] and geometallurgy [22–26] in order to understand the effect of particle behaviour on mineral processing and mining applications.

Liberation spectrum can be estimated by either point/linear (1D), or area (2D), or volumetric (3D) analyses [4,15]. 3D spectrum is collected from bulk samples by using sophisticated methods such as x-ray computerized tomography [27–30]. The commercial application of x-ray tomography is, however, currently scarce and expensive [31]. 1D and 2D spectra, on the other hand, are more commonly used than 3D spectrum. 1D spectrum is obtained by counting points or measuring linear intercept lengths across the area of progeny particles and their constituent mineral phases [15,16,32], whereas the 2D spectrum involves mineralogical mapping of particles on the whole areal section [12]. Both spectra are collected from the surfaces of particles mounted in polished or thin or polished-thin sections. Various stereological procedures have been developed to convert 1D and 2D spectra to 3D spectrum [15,16,33–35], as they might be biased estimates of 3D spectrum [15]; however, such steorological conversions are out of the scope of this research.

1D and 2D spectra can be obtained with scanning electron microscope (SEM)-based tools [24,36] or optical microscopy [37]. Mineral liberation analyzer (MLA) is one of the SEM-based tools which adopts backscattered electron imaging (BSE) and energy-dispersive x-ray spectrometer (EDX) for automated phase discrimination and mineralogical mapping, respectively [16,36,38–40]. Optical microscopes, on the other hand, utilizes visible light and a series of lenses to generate magnified visuals of particles, and a light-sensitive camera to capture those visuals in digital micrographs. These optical micrographs are then evaluated with reliable methods for mineral identification and

* Corresponding author.
E-mail address: mcamalan@metu.edu.tr (M. Camalan).

http://dx.doi.org/10.1016/j.powtec.2017.08.063
0032-5910/

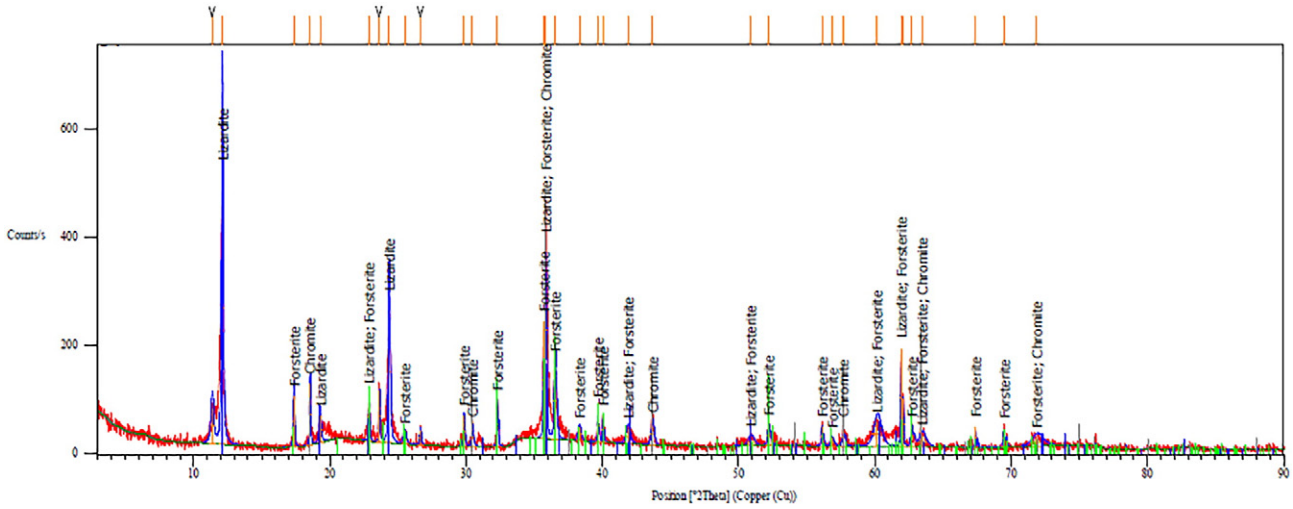

Fig. 1. X-ray diffractrogram of the chromite sample used in this study.

mineralogical mapping. Image processing, in this context, may be used as an automated tool to segment images of rock particles into color channels, each channel representing a different mineral type. It has been used in the fields of geology [41,42], mining [43–47] and mineral processing [3,18,21,25,48–51] for automatic identification or quantification of rock-forming minerals. The basic image processing method for mineral classification is color thresholding as long as the micrographs of minerals have uniquely different color values. However, the micrograph of any mineral might contain different colors because of its texture (e.g. fractures, pits, scratches) or because of the poor acquisition of images by light deficiency. Even the classification will be tedious again if different minerals have uniform yet slightly different color values. Such drawbacks on mineral classification orient researchers to develop more sophisticated ways on image acquisition and/or processing techniques. Examples involve multispectral imaging to discriminate mineral surfaces [18,21,49,51], closed-software routines involving some image operators and color thresholds [3,21,25,50], image classification algorithms such as Naive-Bayes [48] and Process Tree [49]. However, the experimental procedures defined in these studies are either too costly or user-specific, being tedious particularly for the end-users who do not have enough experience in image processing.

The objective of the method presented here is to apply a user-friendly and cost-effective supervised image classification method for the assessment of 2D liberation spectrum through optical micrographs. The 2D spectrum obtained with microscopic analysis was later compared with the one obtained from the MLA. In addition, reproducibility of the proposed method was measured with the replicated classification algorithms. The proposed method was based on estimating mineralogical map of an unknown sample of particles from sample features of the constituent minerals using Random Forest Tree (RFT), a powerful machine-learning algorithm [52,53]. The user, in this case, should only select characteristic sample features of minerals whose statistical properties were extracted by the classifier software. RFT uses these statistical properties in a voting process to classify automatically an unknown image of particles. The strength of this method lies in its feature space which allows the algorithm to evaluate not only the individual colors but also the texture of minerals [54]. Therefore, minerals that even have little color contrast may be classified with RFT by virtue of its texture evaluation, which is not possible with conventional color thresholding. This method has the potential to distinguish various metallic ore minerals from gangue minerals because light interacts with these mineral surfaces in different paths (reflection or refraction), yielding dissimilar textures on micrographs. The misclassification, on the other hand, may occur when the objects have low contrast in texture. Such low contrast has been observed between the surfaces of non-opaque (gangue) minerals and epoxy [21], which may deter the extraction of particles from epoxy by using RFT. Another weakness may arise from user-based selection of sample features, which may introduce bias to the classification. However, the classifier software has a user-friendly interface to edit sample features; thus, any possible bias from feature selection can be minimized [54]. The method might not also classify individual grains whose sizes are near to 0.2 μm, as this is the best theoretical resolution of light microscope [55]. If the trace minerals or rare-earths have such small grain sizes, their classification on micrographs will be problematic. In fact, it is already suggested that image analysis methods on micrographs can be used to determine the quantity of ore minerals down to about 0.1% [16].

Table 1
Semi-quantitative mass distribution of minerals within the experimental material.

Mineral species	Semi-quantitative distribution (%)
Chromite	18
Forsterite	33
Lizardite	49

2. Experimental material and procedure

The experimental sample was a chromite ore within the size range of −600 + 150 μm. The mineral species of the sample were detected with Rigaku Ultima IV X-ray diffractometer (XRD) with a Cu-Kα X-ray tube, operating at 40 kV and 30 mA. The qualitative XRD analysis revealed that the major minerals within the sample are chromite, forsterite and lizardite (Fig. 1 and Table 1).

The MLA analysis was performed on FEI-QUANTA Scanning Electron Microscope adapted with EDAX Genesis XM4i x-ray microanalysis system. Image acquisition and microscopic analysis were accomplished with binocular Wetzlar 21-D6330 reflected microscope attached with Cnscope 5 MP digital CMOS camera. The scale of the image was determined using a micrometer. The polished sections of the experimental sample were prepared in a cold-mounting Epofix resin kit, further ground and polished on a series of diamond and velvet discs using Struers Tegramin 25 equipment. Meanwhile, additional polished sections were prepared from chromite-rich and silicate-rich fractions of the sample separated in the heavy liquid of bromoform. Images of these additional polished sections were used in mineral identification during image classification.

All the image analysis routines were performed in freely-distributed and open-source Fiji-ImageJ software, which is particularly used in life sciences [56]. Meanwhile, the trainable Weka Segmentation toolbox

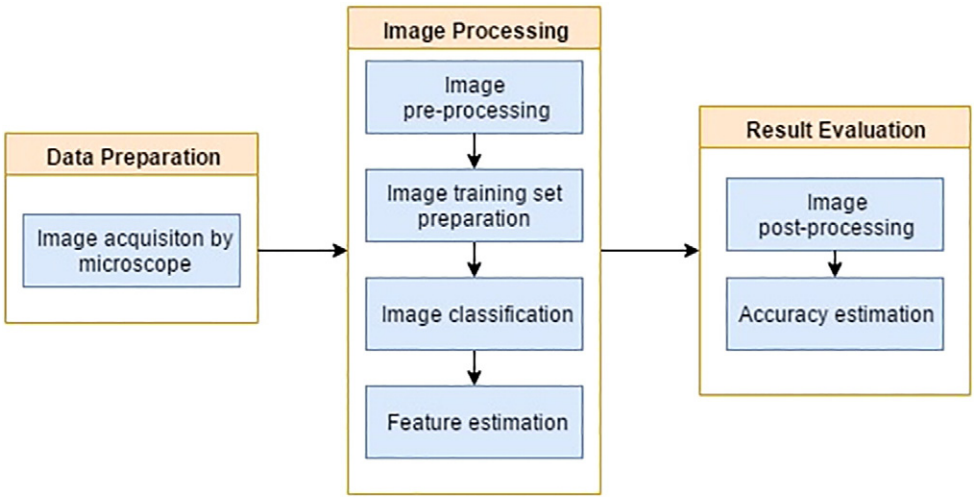

Fig. 2. A schematic diagram showing the stages of image processing for mineral classification.

developed and implemented into Fiji by Arganda-Carreras [54] was used for image classification. The toolbox contains various supervised classification algorithms to segment any unknown image or a stack of images. Besides, the software is capable to classify several image types taken from light or scanning electron microscopes.

2.1. Acquisition of the liberation spectrum from optical micrographs

The methodology used to obtain the liberation spectrum by image analysis consists of (i) pre-processing, (ii) training data extraction, (iii) image classification, (iv) post-processing and evaluation. Fig. 2 shows steps of the image processing methodology.

2.1.1. Image pre-processing

This stage involves firstly removing background (image of epoxy) from particles, and then minimizing the unwanted noise and other artifacts inherent on the images of particles. The former was done by manually selecting and extracting images of particles to a white background, using the blow/lasso tool (Fig. 3). Then, the Kuwahara (Fig. 4a) and the median (Fig. 4b) filters were applied to the epoxy-free images of particles to eliminate noise and other artifacts form the image. The Kuwahara filter is a non-linear smoothing filter used for adaptive noise reduction while keeping the edges of the objects unaffected [57]. Similarly, the median filter is a non-linear technique, in which the pixels are sorted into grids of certain size where the central pixel replaces the median value [58]. For this study, the Kuwahara and the median filters were applied on a 5 × 5 and 3 × 3 pixel sub-regions, respectively.

2.1.2. Training data extraction and sample feature selection

Training sample data was constructed from images of particles taken from chromite-rich and silicate-rich polished sections (Fig. 5). Four classification classes (chromite, lizardite/olivine, unknown, and background) were assigned for the images, and then various sample textures and training features of these classes were selected manually (Fig. 6). The software generates training data to be used on the classification of unknown samples.

2.1.3. Image classification

Image classification was performed using the random-forest tree (RFT) method. The goal was to generate a model predicting the value of a target variable based on several input variables, using individual decision trees (meta-learners) estimated from the sample training data. RFT combined multiple random trees that vote on a particular outcome where each vote is given equal weight. The Forest chooses the classification that contains the most votes. The method offers visualization for high-dimensional data (many columns), clustering, outliers and error detection.

2.1.4. Post-processing and evaluation

Post processing stage involves removing the residual noise and artifacts after image classification. For that purpose, the Kuwahara and the median filters were applied to the classified image, on 5 × 5

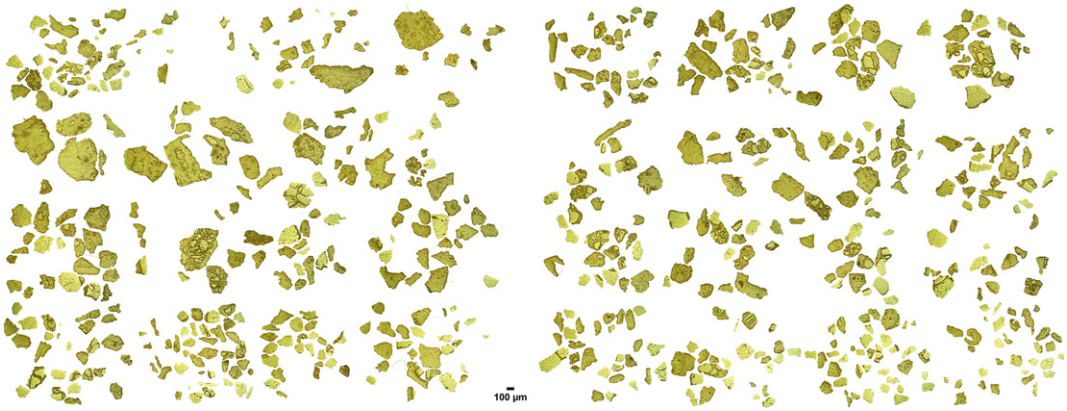

Fig. 3. The raw image of particles manually selected from chromite sample.

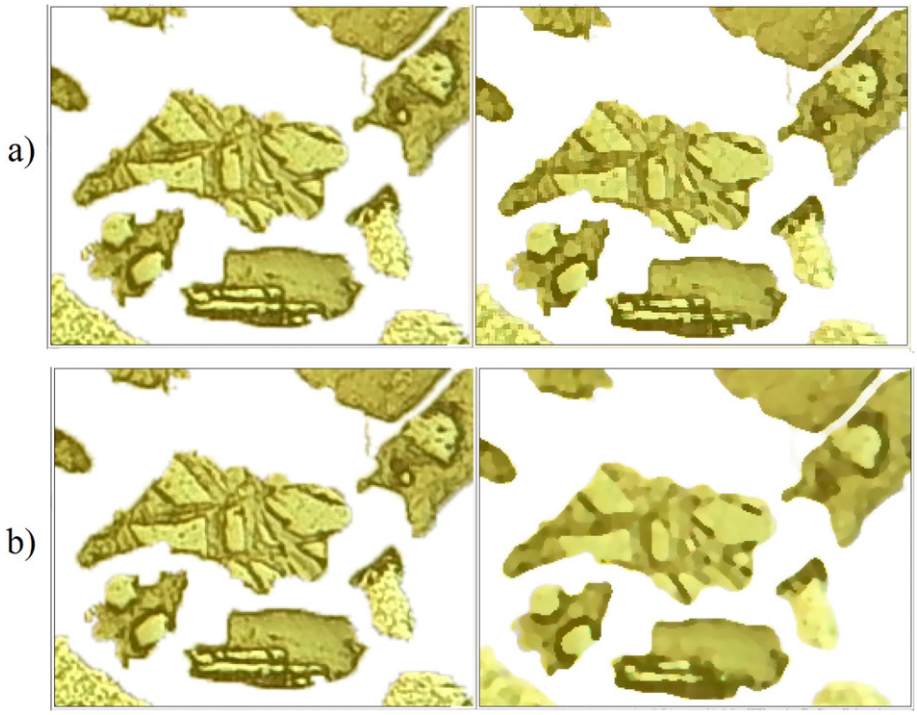

Fig. 4. Illustrative application of (a) Kuwahara Filtering (b) Median Filtering on an arbitrary particle surface.

and 3 × 3 pixel sub-regions respectively. The classified image (Fig. 7) shows well-classified data with respect to the original image, based on visual perception.

Evaluation of the results were achieved with an accuracy assessment method, which is widely used in remote sensing [59–61]. The assessment involved generation of 250 arbitrary yet spatially identical points

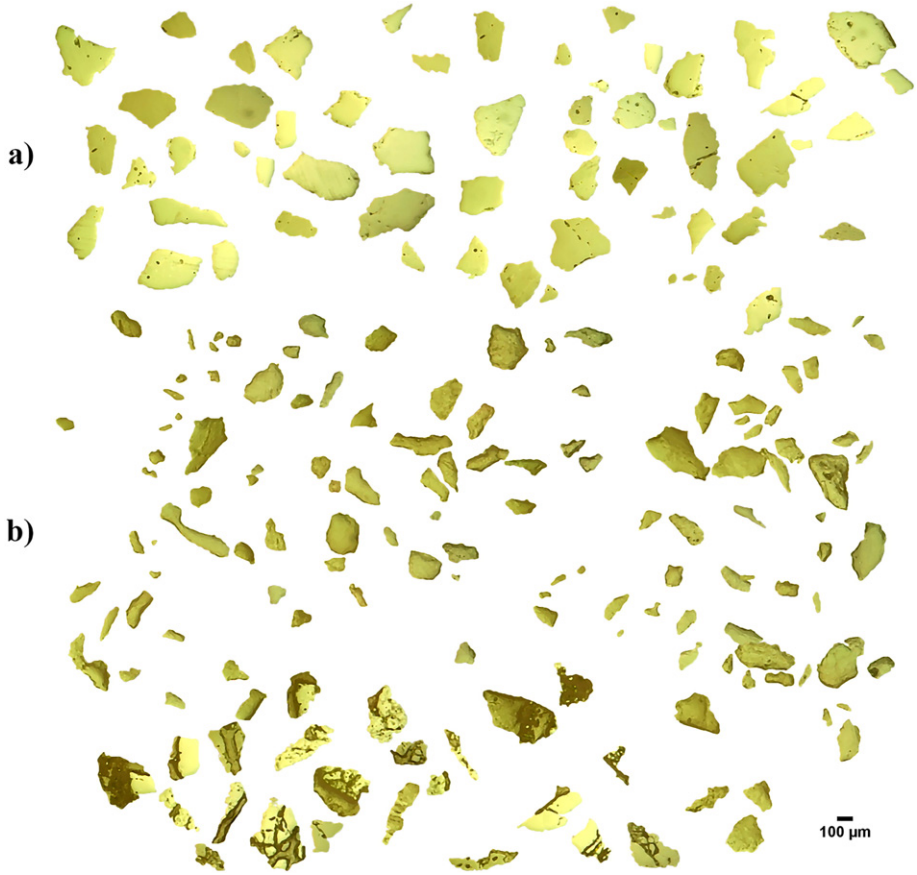

Fig. 5. Surface images of particles taken from (a) chromite-rich, (b) silicate-rich fractions.

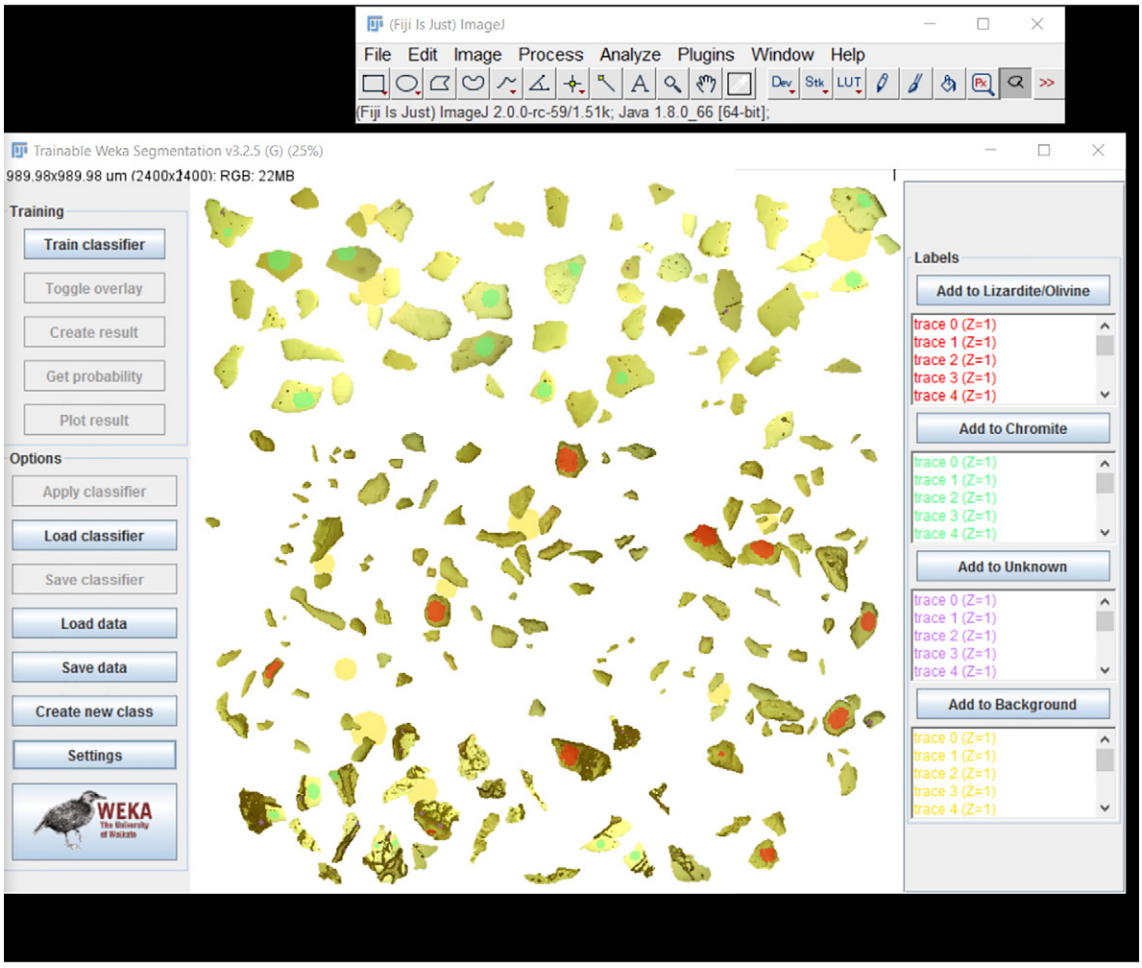

Fig. 6. Selection of sample textures and training features for classification.

on both of the classified (Fig. 7) and original (Fig. 3) images. Then, point-by-point comparison was made between classifier prediction and the true value decided by the user. Meanwhile, the user-bias on the true values was minimized by referring to the pure mineral surfaces of chromite and gangue on the training image (Fig. 5). The point-by-point comparisons were then summarized in an error matrix (Table 2) where diagonals represent correctly classified points. This matrix can be used to determine various indicators for accuracy. Overall accuracy is the number fraction of the correctly classified points (sum of all diagonals) to the total points measured. Another accuracy indicator that is derived from the same data is the Kappa statistic, which is the difference between actual agreement of classification and the agreement by chance, analogous to R-squared value. Although the overall accuracy and the Kappa statistic both give the average error bands for the whole classification process, they do not indicate the error and its source for each mineral class. Errors may arise because of the random-forest classification or the user-dependent feature selection. Error in the former is measured with the producer accuracy, which is the number fraction of correctly classified points of each class in the original image (Fig. 3). Error in the feature selection, on the other hand, is shown with the

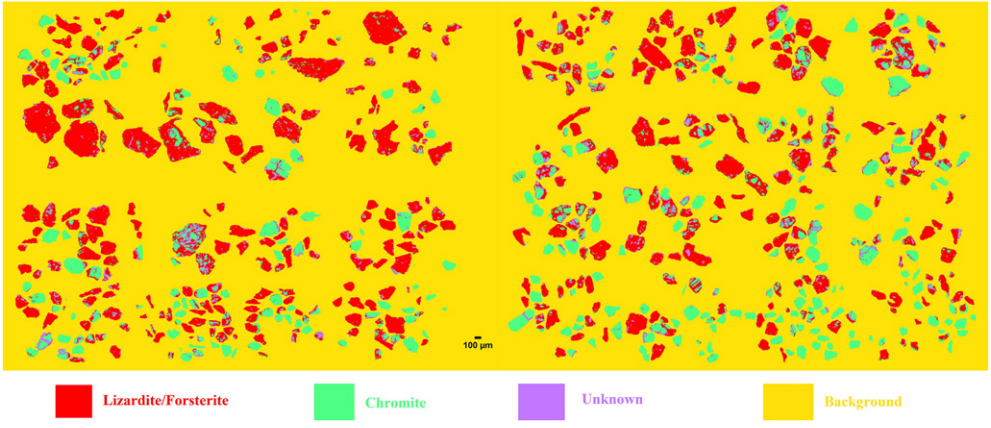

Fig. 7. Final classified image after post-processing.

Table 2
Accuracy assessment and Kappa statistics.

		Class types taken from the reference image (Fig. 3)					
	Class type	Background	Chromite	Lizardite/forsterite	Unknown	Row total	User accuracy
Class types assigned at the classified image (Fig. 7)	**Background**	**12**	0	0	0	12	**1**
	Chromite	0	**92**	3	0	95	**0.97**
	Lizardite/forsterite	0	1	**118**	0	119	**0.99**
	Unknown	0	1	6	**17**	24	**0.71**
	Column total	12	94	127	17	**250**	
	Producer accuracy	**1**	**0.98**	**0.93**	**1**		
	Overall accuracy	***0.96***					
	Kappa statistic	***0.93***					
	Observed agreement	0.96					
	Expected agreement	0.39					

user accuracy, the number fraction of true points of each class in the classified image (Fig. 7). All the abovementioned indicators in Table 2 indicate accurate classification, except for the low user accuracy of unknown class, possibly because of the biased selection of unknown class to the training data set (Fig. 6).

The data for the liberation spectrum were collected by using Clemex Vision software based on a series of simple procedures involving gray thresholding and Boolean operators (Fig. 8). Particle diameters were measured as equivalent circle diameters both in microscopic and MLA analyses. Meanwhile, the areas were both measured in squares of μm. Then, the area-based chromite grade (g_i %) of any particle i was calculated as:

$$g_i = 100 * \left[A_{chr,i}/(A_{chr,i} + A_{gang,i})\right] \quad (1)$$

where $A_{chr,i}$ and $A_{gang,i}$ are the areas of chromite and gangue, respectively, in particle i. Unclassified regions on the mineral map (Fig. 7) were excluded for grade estimation in Eq. (1) because their content had not been identified. The liberation spectrum was constructed by plotting the probability (or cumulative) density function of g_i classes. Meanwhile, grade-recovery curve was constructed by plotting the area-based recovery (%) of the total chromite content to each one-sided g_i class (e.g. >0%, >10%, >95%, etc.).

3. Results and discussion

Fig. 9 shows that the overall mineralogical contents measured with MLA and microscopic analysis are in good agreement. The other minerals (dolomite, calcite, augite, diopside, biotite, hematite, ankerite, zincite, clinochlore and quartz) measured with MLA occupy minor amounts in the experimental sample. Therefore, neglecting these trace minerals in the microscopic analysis would not change the liberation spectrum.

A possibly conflicting result is the discrepancy of the area-based mineral abundances (Fig. 9) from the mass-based mineralogical composition (Table 1). This discrepancy might be expected if the area-based mineralogical map and composition are biased representatives of their mass-based equivalents; however, there is not a consensus in the relevant literature data whether such bias is present [4,29,62,63] or not [35,62]. On the other hand, if we assume surface composition is the unbiased representive of the bulk, the discrepancy might be due to the preferential settling of chromite on the polished surface, which is expected when minerals in the polished section have large differences in density [16,21]. Nevertheless, we cannot conclude why surface compositions measured by MLA and microscopic analysis differ from the bulk composition, given that neither MLA nor microscope gives direct information about the bulk of the sample.

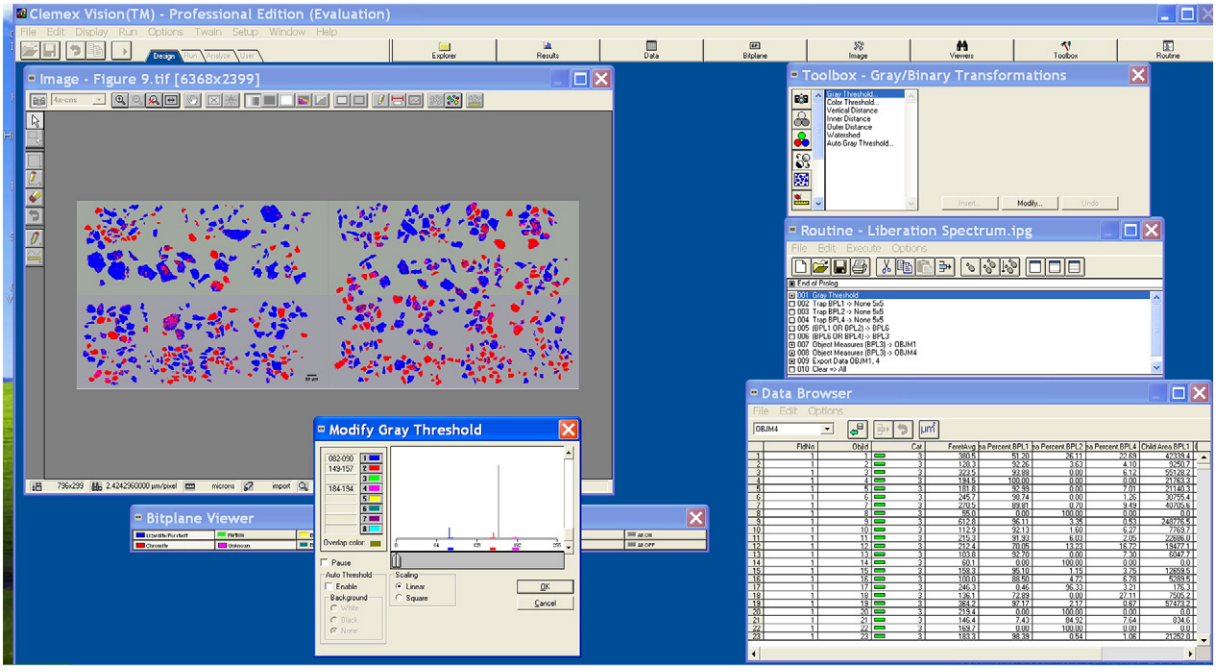

Fig. 8. Acquisition of 2D liberation spectrum on the classified image by a routine of gray thresholding and Boolean operators.

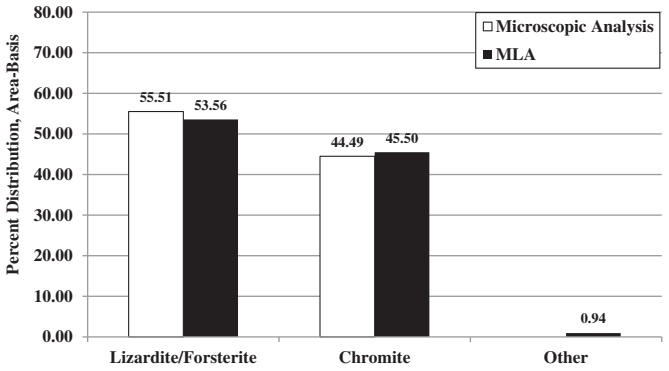

Fig. 9. Overall mineralogical content of the chromite sample measured with MLA and Microscopic Analysis.

Based on the relative abundance of grade classes, the spectra of microscopic analysis and MLA seem to be consistent (Fig. 10). However, microscopic analysis predicts the middling content more than MLA does, causing a substantial decrease in the measurement of the liberated gangue (0–10%). As a result, microscopic analysis estimates a grade-recovery curve which shows poorer liberation (Fig. 11). The reasons why microscopic analysis estimates poor liberation than MLA might be linked to its biased population and/or residual noise (misclassified minerals) generated by RFT. The former is inevitable since, unlike MLA, the sample for the microscopic analysis was manually selected. Such a manual selection would bring out a biased population in which the amount of fine particles are underestimated (Fig. 12). Then, the absence of fine particles may alter the resultant spectrum if the spectrum varies with particle size. To observe the variation of the spectrum with particle size, the spectra of three size classes (−300/+212 μm, −212/+150 μm and −150/+106 μm) from the whole sample were extracted by microscopic analysis and MLA. These size classes were selected because they occupy nearly the same frequency in both measurement methods (Fig. 12), eliminating the effect of biased selection on the liberation spectrum. Results show that neither method estimates a variation of the spectrum with particle size (Figs. 13, 14 and 15), indicating no correlation between sample selection and liberation spectrum. Meanwhile, in each of these size classes, microscopic analysis demonstrated higher middling content with a decrease in liberated gangue. This characteristic change indicates that the residual noise left on the surfaces of lizardite/forsterite causes to underestimate chromite liberation (Fig. 11) by misgrading liberated lizardite/forsterite particles as middling (Fig. 10). Nevertheless, we cannot conclude if the residual noise causes the resultant spectrum and grade-recovery curve to diverge from their true values since the accuracy indicators in microscopic analysis are still high (Table 2). We could not even conclude if MLA is more accurate than the microscopic analysis due to the lack of standard procedures on reference mineral surfaces to quantify the accuracy and precision of MLA [39].

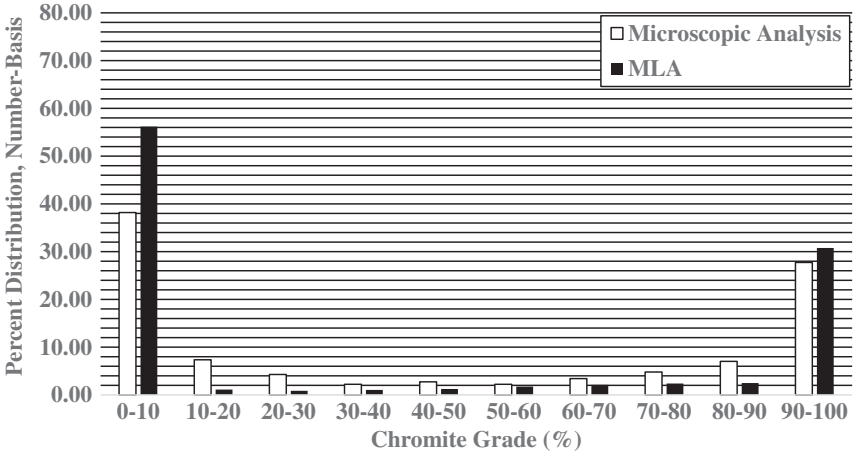

Fig. 10. Liberation Spectra obtained with microscopic analysis and MLA.

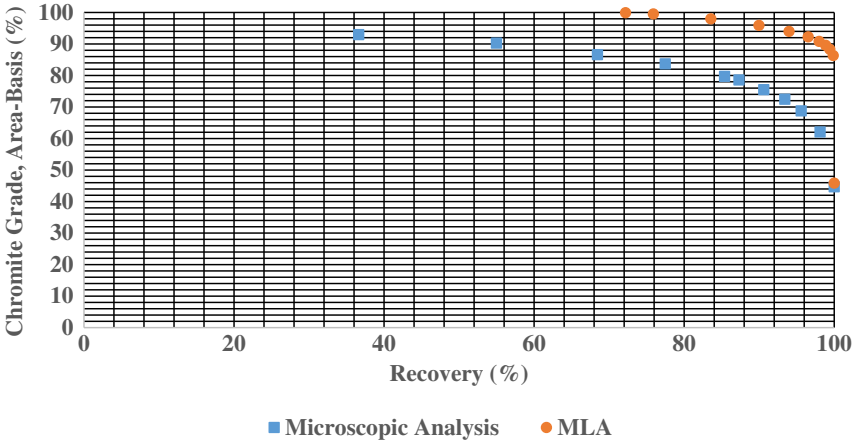

Fig. 11. Grade-recovery curves obtained with microscopic analysis and MLA.

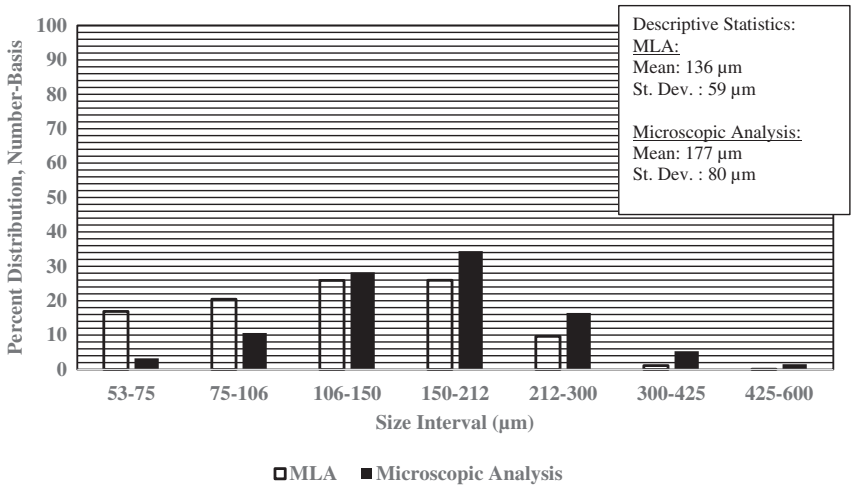

Fig. 12. Size (equivalent circle diameter) distribution of the experimental sample measured with MLA and microscopic Analysis.

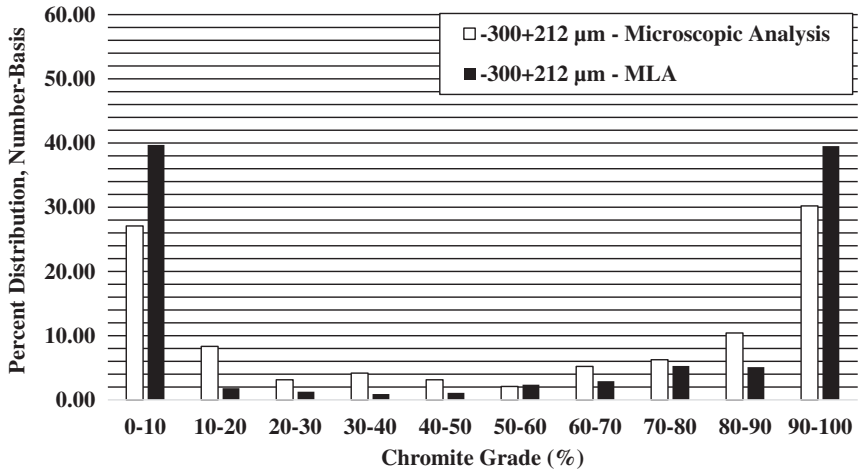

Fig. 13. Liberation spectra of −300 + 212 µm size fraction obtained with microscopic analysis and MLA.

In the case of microscopic analysis, it was of interest to measure the variation of the measured spectrum, mineralogical composition and grade-recovery curve with the number of particles that are randomly selected for analysis so that a sufficiently small sample size could be determined for a statistically meaningful analysis. For this purpose, sub-samples having different number of particles were randomly

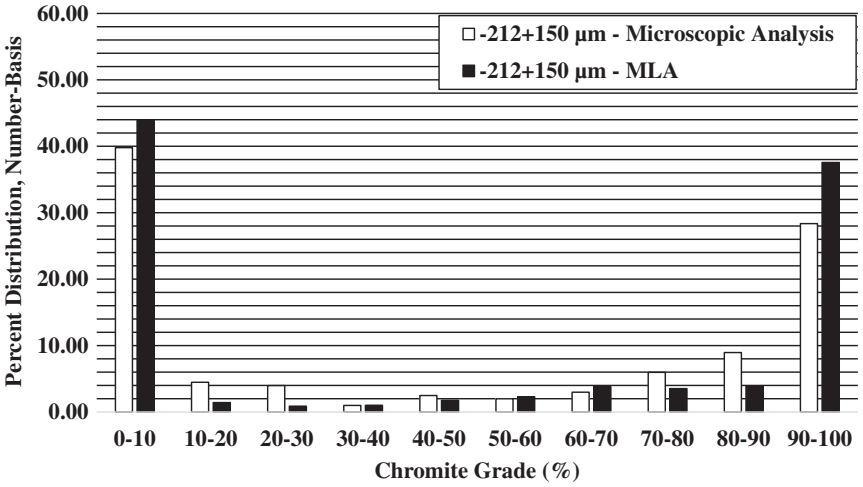

Fig. 14. Liberation spectra of −212 + 150 µm size fraction obtained with microscopic analysis and MLA.

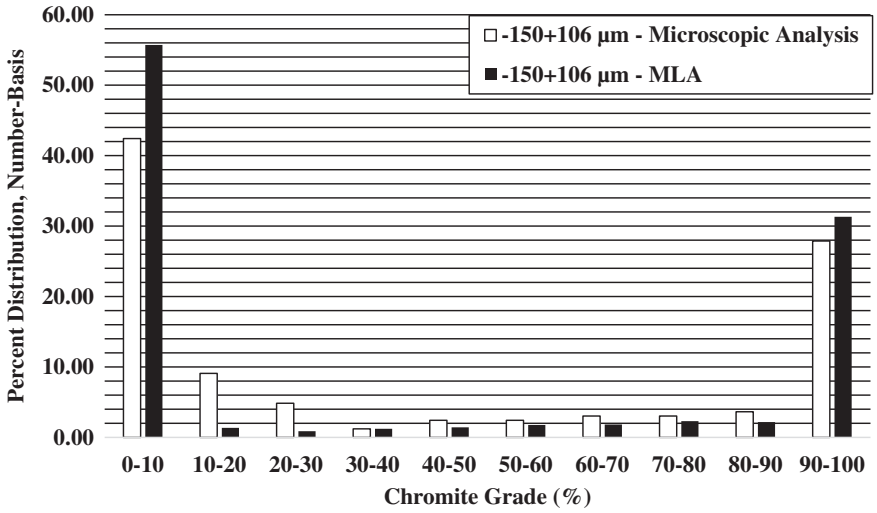

Fig. 15. Liberation spectra of −150 + 106 µm size fraction obtained with microscopic analysis and MLA.

selected from the original image (Fig. 7). It is clear from Figs. 16–18 that a sub-sample with 200 particles would be sufficient for the tested ore sample to reproduce data for its liberation spectrum (Fig. 16), mineralogical composition (Fig. 17) and grade-recovery curve (Fig. 18). This finding was also statistically supported by the chi-square goodness-of-fit test that was applied to the liberation spectra of the sub-samples with 50, 100, 200, and 400 particles to check if their spectra are statistically different or not from the spectrum of the whole sample containing 590 particles. The test results are summarized in Table 3. The *P* values of the test for sub-samples including 200 and 400 particles are too large to reject the null hypothesis that their spectra are statistically different than the spectrum of the whole sample. This allows us to conclude that the sub-sample size for this test sample (Fig. 7) should be no <200 particles. For any other rock samples, sub-samples larger than 200 particles may be required to reproduce liberation spectrum, especially if its constituent minerals have lower grades and/or finer grain sizes. In fact, Vigneau et al. [64] showed that 500 particles are required to assess reasonable precision in the size distribution of very-fine granules (with a median around 10 µm) under microscope. Assuming precise size distribution ensures precise mineralogical map, 500 particles at most will be sufficient to reproduce liberation spectrum, regardless of the grain sizes of minerals.

4. Conclusion

Supervised image classification in microscopic analysis can be easily used to generate an accurate 2D mineral map of chromite samples from which 2D liberation spectrum can be extracted. This classification algorithm and its associated software can be used without getting involved with the intricacies of image processing as the software has an open-source and user-friendly environment. The proposed classification algorithm (Random Forest Tree) is capable to evaluate the texture of mineral surfaces, unlike color thresholding, which makes it a potential candidate to distinguish metallic ore minerals from gangue minerals.

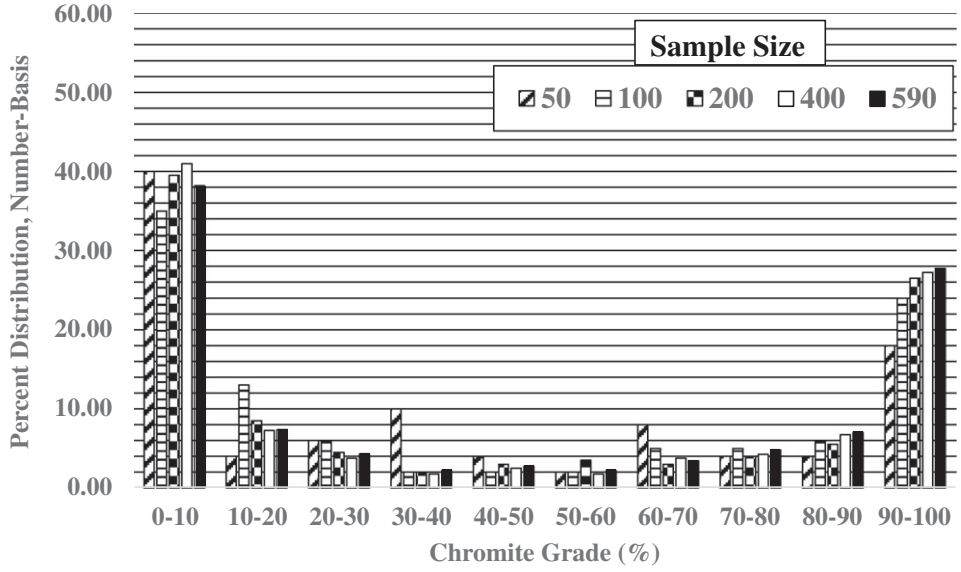

Fig. 16. Spectrum measurements with different sample sizes.

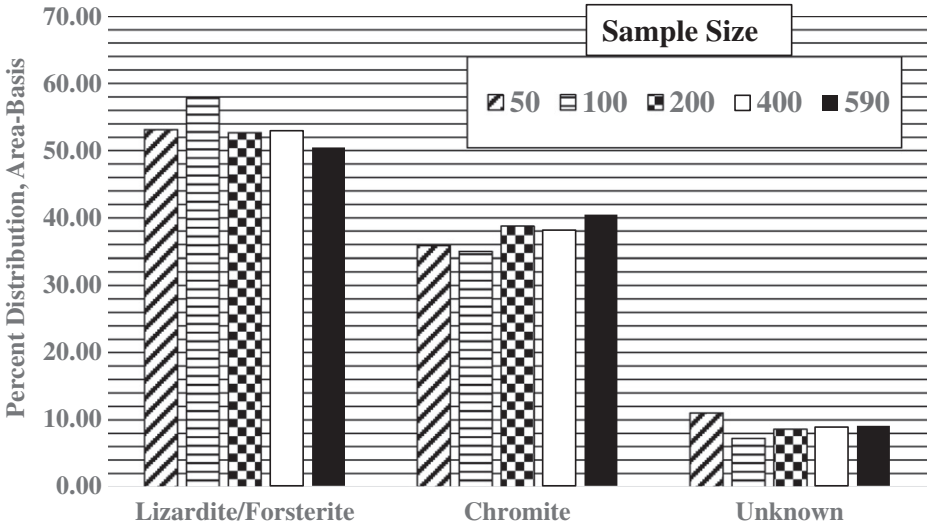

Fig. 17. Measurements of the mineralogical composition with different sample sizes.

Using the proposed microscopic analysis method, area-based liberation spectrum, mineralogical composition and grade-recovery curve of this particular chromite sample could be reproduced with a minimum sample size of 200 particles randomly selected from the original micrographs. This population size, however, may vary for other ore samples, depending on the grade and grain size distribution of their constituent minerals.

The mineralogical composition of the sample obtained by the microscopic method agreed quite well with that obtained by the MLA method. However, the mineral spectrum and grade-recovery curves obtained by the microscopic method predicted poorer liberation than MLA does. One reason for this could be the residual noise on gangue (lizardite/olivine) surfaces generated by the Random Forest classification, particularly misgrading of liberated gangue into middlings. Nevertheless, we cannot compare the reliabilities of the two methods since there is not any standard procedure on reference mineral surfaces to quantify the accuracy of MLA. Then, the comparison of the reliabilities of the two methods should be the subject of further research.

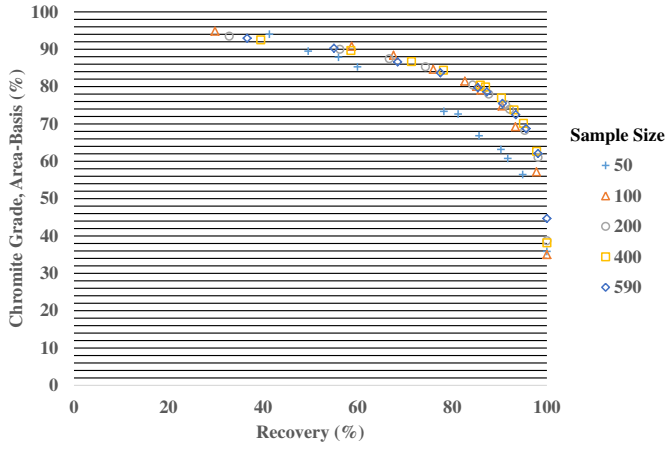

Fig. 18. Measurements of the grade-recovery curves with different sample sizes.

Table 3
The indicators of chi-square goodness-of-fit test on the liberation spectra of sub-samples.

Population size of sub- samples	Reference sample (Population size: 590)	
	Chi-square statistic	P-value
50	20.5141	0.015
100	6.90236	0.647
200	3.15584	0.958
400	2.44592	0.982

Acknowledgements

The authors would like to thank Dr. N. Metin Can and Dr. İlkay B. Çelik from Hacettepe Technical University for their valuable support and help regarding the preparation of polished sections in their laboratory. This work was partially supported by the BAP institutional fund of the Middle East Technical University [grant number BAP-07-02-2014-007-466].

References

[1] N.O. Lotter, L.J. Kormos, J. Oliveira, D. Fragomeni, E. Whiteman, Modern process mineralogy: two case studies, Miner. Eng. 24 (2011) 638–650, http://dx.doi.org/10.1016/j.mineng.2011.02.017.
[2] R.D. Pascoe, M.R. Power, B. Simpson, QEMSCAN analysis as a tool for improved understanding of gravity separator performance, Miner. Eng. 20 (2007) 487–495, http://dx.doi.org/10.1016/j.mineng.2006.12.012.
[3] I.B. Celik, N.M. Can, J. Sherazadishvili, Influence of process mineralogy on improving metallurgical performance of a flotation plant, Miner. Process. Extr. Metall. Rev. 32 (2010) 30–46, http://dx.doi.org/10.1080/08827508.2010.509678.
[4] M.I. Al-Wakeel, C.L. Lin, J.D. Miller, Significance of liberation characteristics in the fatty acid flotation of Florida phosphate rock, Miner. Eng. 22 (2009) 244–253, http://dx.doi.org/10.1016/j.mineng.2008.07.011.
[5] J. Quinteros, E. Wightman, N.W. Johnson, D. Bradshaw, Evaluation of the response of valuable and gangue minerals on a recovery, size and liberation basis for a low-grade silver ore, Miner. Eng. 74 (2015) 150–155, http://dx.doi.org/10.1016/j.mineng.2014.12.019.
[6] E. Donskoi, S.P. Suthers, J.J. Campbell, T. Raynlyn, Modelling and optimization of hydrocyclone for iron ore fines beneficiation - using optical image analysis and iron ore texture classification, Int. J. Miner. Process. 87 (2008) 106–119, http://dx.doi.org/10.1016/j.minpro.2008.02.006.
[7] G. Barbery, Liberation 1, 2, 3: theoretical analysis of the effect of space dimension on mineral liberation by size reduction, Miner. Eng. 5 (1992) 123–141, http://dx.doi.org/10.1016/0892-6875(92)90038-B.
[8] A.M. Gaudin, Liberation, Princ. Miner. Dress, McGraw-Hill Book Company, Inc., New York 1939, pp. 70–91.
[9] R.P. King, A model for the quantitative estimation of mineral liberation by grinding, Int. J. Miner. Process. 6 (1979) 207–2207.
[10] T.P. Meloy, Liberation theory — eight, modern, usable theorems, Int. J. Miner. Process. 13 (1984) 313–324http://dx.doi.org/10.1016/0301-7516(84)90051-6.

[11] C.L. Schneider, Measurement and Calculation of Liberation in Continuous Milling Circuit, The University of Utah, 1995http://dx.doi.org/10.1017/CBO9781107415324.004.
[12] E.M. Wightman, C.L. Evans, Representing and interpreting the liberation spectrum in a processing context, Miner. Eng. 61 (2014) 121–125, http://dx.doi.org/10.1016/j.mineng.2013.12.012.
[13] T. Leißner, T. Mütze, K. Bachmann, S. Rode, J. Gutzmer, U.A. Peuker, Evaluation of mineral processing by assessment of liberation and upgrading, Miner. Eng. 53 (2013) 171–173, http://dx.doi.org/10.1016/j.mineng.2013.07.018.
[14] R.P. King, Comminution operations, Model. Simul. Miner. Process. Syst, Butterworth-Heinmann Publications, Oxford 2001, pp. 127–210.
[15] G.M. Leigh, G.J. Lyman, P. Gottlieb, Stereological estimates of liberation from mineral section measurements: a rederivation of Barbery's formulae with extensions, Powder Technol. 87 (1996) 141–152, http://dx.doi.org/10.1016/0032-5910(95)03080-8.
[16] W. Petruk, Applied Mineralogy in the Mining Industry, 1st ed. Elsevier, Ottawa, 2000.
[17] G.J. Lyman, Method for interpolation of 2-D histogram data: application to mineral liberation data, Powder Technol. 83 (1995) 133–138, http://dx.doi.org/10.1016/0032-5910(94)02949-O.
[18] J. Hunt, R. Berry, D. Bradshaw, Characterising chalcopyrite liberation and flotation potential: examples from an IOCG deposit, Miner. Eng. 24 (2011) 1271–1276, http://dx.doi.org/10.1016/j.mineng.2011.04.016.
[19] K. Tungpalan, E. Wightman, E. Manlapig, Relating mineralogical and textural characteristics to flotation behaviour, Miner. Eng. 82 (2015) 136–140, http://dx.doi.org/10.1016/j.mineng.2015.02.005.
[20] E. Whiteman, N.O. Lotter, S.R. Amos, Process mineralogy as a predictive tool for flowsheet design to advance the Kamoa project, Miner. Eng. 96–97 (2016) 185–193, http://dx.doi.org/10.1016/j.mineng.2016.05.004.
[21] G.R. Lane, C. Martin, E. Pirard, Techniques and applications for predictive metallurgy and ore characterization using optical image analysis, Miner. Eng. 21 (2008) 568–577, http://dx.doi.org/10.1016/j.mineng.2007.11.009.
[22] C. Lund, P. Lamberg, T. Lindberg, Development of a geometallurgical framework to quantify mineral textures for process prediction, Miner. Eng. 82 (2015) 61–77, http://dx.doi.org/10.1016/j.mineng.2015.04.004.
[23] K. Tungpalan, E. Manlapig, M. Andrusiewicz, L. Keeney, E. Wightman, M. Edraki, An integrated approach of predicting metallurgical performance relating to variability in deposit characteristics, Miner. Eng. 71 (2015) 49–54, http://dx.doi.org/10.1016/j.mineng.2014.10.004.
[24] J. Zhou, Y. Gu, Geometallurgical characterization and automated mineralogy of gold ores, in: M.D. Adams (Ed.), Gold Ore Process, 2nd ed.Elsevier 2016, pp. 95–111, http://dx.doi.org/10.1016/B978-0-444-63658-4.00006-2.
[25] I.D. Delbem, R. Galéry, P.R.G. Brandão, A.E.C. Peres, Semi-automated iron ore characterisation based on optical microscope analysis: quartz/resin classification, Miner. Eng. 82 (2015) 2–13, http://dx.doi.org/10.1016/j.mineng.2015.07.021.
[26] C. Philander, A. Rozendaal, The application of a novel geometallurgical template model to characterise the Namakwa Sands heavy mineral deposit, West Coast of South Africa, Miner. Eng. 52 (2013) 82–94, http://dx.doi.org/10.1016/j.mineng.2013.04.011.
[27] C.L. Lin, J.D. Miller, Cone beam X-ray microtomography for three-dimensional liberation analysis in the 21st century, Int. J. Miner. Process. 47 (1996) 61–73.
[28] R.A. Mariano, Measurement and Modelling of the Liberation and Distribution of Minerals in Comminuted Ores, The University of Queensland, 2016.
[29] J.F. Medina, Liberation-Limited Grade/Recovery Curves for Auriferous Pyrite Ores as Determined by High Resolution X-ray Microtomography, The University of Utah, 2012.
[30] G. Schena, L. Santoro, S. Favretto, Conceiving a high resolution and fast X-ray CT system for imaging fine multi-phase mineral particles and retrieving mineral liberation spectra, Int. J. Miner. Process. 84 (2007) 327–336, http://dx.doi.org/10.1016/j.minpro.2006.10.002.
[31] J. Zhang, N. Subasinghe, Prediction of mineral liberation characteristics of comminuted particles of high grade ores, Miner. Eng. 49 (2013) 68–76, http://dx.doi.org/10.1016/j.mineng.2013.05.005.
[32] M.M. Minnis, An automatic point-counting method for mineralogical assessment, Am. Assoc. Pet. Geol. Bull. 68 (744–752) (1984) 744–752.
[33] R.P. King, Comminution and liberation of minerals, Miner. Eng. 7 (1994) 129–140.
[34] R.P. King, C.L. Schneider, An effective Sem-based image analysis system for quantitative mineralogy, KONA Powder Part. J. 11 (1993) 165–177.
[35] D. Lätti, B.J.I. Adair, An assessment of stereological adjustment procedures, Miner. Eng. 14 (2001) 1579–1587, http://dx.doi.org/10.1016/S0892-6875(01)00176-5.
[36] R. Fandrich, Y. Gu, D. Burrows, K. Moeller, Modern SEM-based mineral liberation analysis, Int. J. Miner. Process. 84 (2007) 310–320, http://dx.doi.org/10.1016/j.minpro.2006.07.018.
[37] J.R. Craig, D.J. Vaughan, Ore Microscopy and Ore Petrography, 2nd ed. John Wiley & Sons, New York, 1994.
[38] Y. Gu, Automated scanning electron microscope based mineral liberation analysis, J. Miner. Mater. Charact. Eng. 2 (2003) 33–41.
[39] P.J. Sylvester, Use of the Mineral Liberation Analyzer (MLA) for Mineralogical Studies of Sediments and Sedimentary Rocks, Quant. Mineral. Microanal. Sediments Sediment. Rocks, Mineralogical Association of Canada Short Course Series, vol. 42, 2012 1–16.
[40] T.G. Vizcarra, E.M. Wightman, N.W. Johnson, E.V. Manlapig, The effect of breakage mechanism on the mineral liberation properties of sulphide ores, Miner. Eng. 23 (2010) 374–382, http://dx.doi.org/10.1016/j.mineng.2009.11.012.
[41] T.R. Mengko, Y. Susilowati, R. Mengko, B.E. Leksono, Digital image processing technique in rock forming minerals identification, IEEE APCCAS 2000, 2000 IEEE Asia-Pacific Conf. Circuits Syst. Electron. Commun. Syst. (Cat. No.00EX394) 2000, pp. 441–444, http://dx.doi.org/10.1109/APCCAS.2000.913531.
[42] N. Singh, T. Singh, A. Tiwary, K. Sarkar, Textural identification of basaltic rock mass using image processing and neural network, Comput. Geosci. 14 (2010) 301–310, http://dx.doi.org/10.1007/s10596-009-9154-x.
[43] S. Chatterjee, A. Bhattacherjee, B. Samanta, S.K. Pal, Image-based quality monitoring system of limestone ore grades, Comput. Ind. 61 (2010) 391–408, http://dx.doi.org/10.1016/j.compind.2009.10.003.
[44] W. Wang, Rock particle image segmentation and systems, in: P.-Y. Yin (Ed.), Pattern Recognit. Tech. Technol. Appl, In-Tech, Crotia 2008, pp. 197–226.
[45] D.P. Mukherjee, Y. Potapovich, I. Levner, H. Zhang, Ore image segmentation by learning image and shape features, Pattern Recogn. Lett. 30 (2009) 615–622, http://dx.doi.org/10.1016/j.patrec.2008.12.015.
[46] C.A. Perez, P.A. Estévez, P.A. Vera, L.E. Castillo, C.M. Aravena, D.A. Schulz, L.E. Medina, Ore grade estimation by feature selection and voting using boundary detection in digital image analysis, Int. J. Miner. Process. 101 (2011) 28–36, http://dx.doi.org/10.1016/j.minpro.2011.07.008.
[47] V. Singh, S.M. Rao, Application of image processing in mineral industry: a case study of ferruginous manganese ores, Miner. Process. Extr. Metall. (Trans. Inst. Min Met. C) 115 (2006) 155–160, http://dx.doi.org/10.1179/174328506X109130.
[48] C. Köse, İ. Alp, C. İkibaş, Statistical methods for segmentation and quantification of minerals in ore microscopy, Miner. Eng. 30 (2012) 19–32, http://dx.doi.org/10.1016/j.mineng.2012.01.008.
[49] J. Hunt, R. Berry, S. Walters, Using mineral maps to rank potential processing behaviour, 25th Int. Miner. Process. Congr, Australasian Institute of Mining and Metallurgy, Brisbane 2010, pp. 2899–2905.
[50] E. Donskoi, S.P. Suthers, S.B. Fradd, J.M. Young, J.J. Campbell, T.D. Raynlyn, J.M.F. Clout, Utilization of optical image analysis and automatic texture classification for iron ore particle characterisation, Miner. Eng. 20 (2007) 461–471, http://dx.doi.org/10.1016/j.mineng.2006.12.005.
[51] E. Pirard, S. Lebichot, W. Krier, Particle texture analysis using polarized light imaging and grey level intercepts, Int. J. Miner. Process. 84 (2007) 299–309, http://dx.doi.org/10.1016/j.minpro.2007.03.004.
[52] L. Breiman, Random forests, Mach. Learn. 45 (2001) 5–32, http://dx.doi.org/10.1023/A:1010933404324.
[53] J.J. Huang, W.C. Siu, T.R. Liu, Fast image interpolation via random forests, IEEE Trans. Image Process. 24 (2015) 3232–3245, http://dx.doi.org/10.1109/TIP.2015.2440751.
[54] I. Arganda-Carreras, V. Kaynig, J. Schindelin, A. Cardona, H.S. Seung, Trainable Weka Segmentation: A Machine Learning Tool for Microscopy Image Segmentation, Neurosci. 2014 Short Course 2 - Adv. Brain-Scale, Autom. Anat. Tech. Neuronal Reconstr. Tract Tracing, Atlasing, 2014 73–80.
[55] Y. Leng, Light microscopy, Mater. Charact. Introd. to Microsc. Spectrosc. Methods, John Wiley & Sons (Asia) Pte Ltd., Singapore 2008, pp. 1–44, http://dx.doi.org/10.1007/978-1-4939-6810-7.
[56] R. Lind, Open source software for image processing and analysis: picture this with ImageJ, in: L. Harland, M. Forster (Eds.), Open Source Softw. Life Sci. Res, Woodhead Publishing Limited 2012, pp. 131–149, http://dx.doi.org/10.1533/9781908818249.131.
[57] K. Bartyzel, Adaptive Kuwahara filter, SIViP 10 (2016) 663–670, http://dx.doi.org/10.1007/s11760-015-0791-3.
[58] F. Khorram, H. Memarian, B. Tokhmechi, Limestone chemical components estimation using image processing and pattern recognition techniques, J. Min. Environ. 2 (2011) 126–135.
[59] R.G. Congalton, K. Green, Assessing the Accuracy of Remotely Sensed Data: Principles and Practices, Lewis Publishers, Boca Raton, 1999.
[60] D. Gómez, J. Montero, Determining the accuracy in image supervised classification problems, Proc. 7th Conf. Eur. Soc. Fuzzy Log. Technol 2011, pp. 342–349, http://dx.doi.org/10.2991/eusflat.2011.103.
[61] A. Bogoliubova, P. Tymków, Accuracy assessment of automatic image processing for land cover classification of St. Petersburg protected area, Acta Sci. Pol. 13 (2014) 5–22.
[62] M. Parian, P. Lamberg, R. Möckel, J. Rosenkranz, Analysis of mineral grades for geometallurgy: combined element-to-mineral conversion and quantitative X-ray diffraction, Miner. Eng. 82 (2015) 25–35, http://dx.doi.org/10.1016/j.mineng.2015.04.023.
[63] M. Gräbner, E. Lester, Proximate and ultimate analysis correction for kaolinite-rich Chinese coals using mineral liberation analysis, Fuel 186 (2016) 190–198, http://dx.doi.org/10.1016/j.fuel.2016.08.074.
[64] E. Vigneau, C. Loisel, M.F. Devaux, P. Cantoni, Number of particles for the determination of size distribution from microscopic images, Powder Technol. 107 (2000) 243–250, http://dx.doi.org/10.1016/S0032-5910(99)00192-8.

Mahmut Camalan received his BSc (2009) and MSc degree (2012) in mining engineering from the Middle East Technical University, Ankara, Turkey. Currently, he is a PhD candidate and a research assistant at the same department of the same university. His research interests include physico-chemical aspects of grinding, process mineralogy, population balance modelling in ball mill and hybrid HPGR-ball mill circuits, microwave-assisted breakage of rocks, impact mechanics, and discrete element method.

Mahmut Çavur received the BSc degree in Mining Engineering from Middle East Technical University (METU), Ankara, Turkey. He received MSc degree in Management Information System from Boğaziçi University, İstanbul, Turkey. He received his PhD in Geodetic and Geographic Information Technology from METU, Ankara. He is now continuing MBA at Hasan Kalyoncu University, Gaziantep, Turkey. His research interests include wireless sensor networks, communication networks, image processing, geospatial data analysis and big data.

Çetin Hoşten holds degrees of BSc (1973) and MSc (1976) in mining engineering from the Middle East Technical University, Ankara, Turkey, where he is currently a professor. He obtained his PhD in mineral processing from University of California, Berkeley, in 1982. His teaching and research interests are mainly in the field of mineral processing, particularly ore and cement grinding, and solid/liquid separation.